



Dynamic Ocean Topography of the Greenland Sea: A comparison between satellite altimetry and ocean modeling

Felix L. Müller¹, Claudia Wekerle², Denise Dettmering¹, Marcello Passaro¹, Wolfgang Bosch¹, and Florian Seitz¹

¹Deutsches Geodätisches Forschungsinstitut, Technische Universität München, Arcisstraße 21, 80333 Munich, Germany

²Climate Dynamics, Alfred Wegener Institute, Helmholtz Centre for Polar and Marine Research, Bussestraße 24, 27570 Bremerhaven, Germany

Correspondence: Felix L. Müller (felix-lucian.mueller@tum.de)

Abstract.

The dynamic ocean topography (DOT) in the polar seas can be described by satellite altimetry sea surface height observations combined with geoid information and by ocean models. The altimetry observations are characterized by an irregular sampling and seasonal sea-ice coverage complicating reliable DOT estimations. Models display various spatio-temporal resolutions, but are limited to their computational and mathematical context and introduced forcing models. In the present paper, ALES+ retracked altimetry ranges and derived along-track DOT heights of ESA's Envisat and water heights of the Finite Element Sea-ice Ocean Model (FESOM) are compared to investigate similarities and discrepancies. The study period covers the years 2003-2009. An assessment analysis regarding seasonal DOT variabilities shows good accordance and confirms the most dominant impact of the annual signal in both datasets. A comparison based on estimated regional annual signal components shows 2-3 times stronger amplitudes of the observations but good agreement of the phase. Reducing both datasets by constant offsets and the annual signal reveals small regional residuals and highly correlated DOT time series (correlation coefficient at least 0.67). The highest correlations can be found in areas that are ice-free and affected by ocean currents. However, differences are visible in sea-ice covered shelf regions. Furthermore, remaining constant artificial elevations in the observational data can be addressed to an insufficient representation of the used geoid. In general, the comparison results in good accordance between simulated and altimetry based description of the DOT in the Greenland Sea. Furthermore, the investigation shows that combining both datasets and exploiting the advantages of along-track altimetry observations and those of homogeneous modeled DOT representations leads to a deeper comprehension of the Arctic Ocean's DOT.

1 Introduction

Observing the dynamic ocean topography (DOT) enables the investigation of important oceanic variables. Variations in the DOT are an indicator of changes in the ocean circulation, freshwater inflow, the major current pathways or water mass redistribution. Knowledge about the Arctic water mass distribution and ocean transport variability is essential to understand and quantify changes in the global overturning circulation system (e.g. Johannessen et al. (2014), Morison et al. (2012)). These re-



relationships led to studies and expeditions since the early 20th century, e.g. by Helland-Hansen and Nansen (1909) investigating the north polar circulation.

Nowadays, satellite altimetry in connection with knowledge about the geoid is one possibility to provide instantaneous DOT snapshots on a global scale. However, in polar regions, altimetry observations obey an irregular sampling in seasonally sea-ice covered regions. Nevertheless, the launch of ESA's earth observation satellite ERS-1 in 1991 constituted the starting point of regular observed DOT information in the higher latitudes for more than 25 years. Followed by regularly improved radar altimetry as well as significant progress in gravity field missions (e.g. GOCE and GRACE), remote sensing missions provided increasingly reliable DOT estimates. Beside an expanded remote Earth observation mission constellation, also advances in data processing (e.g. Laxon (1994), Peacock (2004), Connor et al. (2009)) contributed to an increasing accuracy of DOT heights mainly by improving radar echoes processing strategies (e.g. use of high-frequency data, enhanced retracking and radar echo classification algorithms).

Arctic DOT information for different periods and with different spatial resolutions has been estimated for example by Kwok and Morison (2011) based on laser altimetry or by Farrell et al. (2012) based on a combination of laser and radar altimetry. Moreover, Armitage et al. (2016) processed monthly altimetry derived DOT outputs to combine them with GRACE ocean mass products. However, all these DOT results are based on grid processing with limited spatio-temporal resolutions leading to unavoidable smoothing effects and leaving space for further DOT product improvements.

Beside the observational database, model simulations have provided a variety of different climate variables in polar regions for more than 60 years (Koldunov et al. (2014)). They are characterized by various spatio-temporal resolutions and simulation strategies. In spite of to difficult observation conditions at the high-latitudes, models enable comprehensive analyses of interactions between the Arctic Ocean and atmospheric circulations. However, different models show significant discrepancies related to their fundamental outputs, e.g. sea-surface variability or ocean currents (Koldunov et al. (2014)). Nevertheless, in contrast to satellite altimetry, models provide spatial homogeneous and temporal complete sea surface estimates. In order to get an impression on the model accuracies, previous studies, for example Koldunov et al. (2014), performed an intercomparison of different ocean models, tide gauge observations and weekly averaged altimetry DOT data in the Arctic environment, limited however to gridded DOT data originating of sea-ice free month. The authors conclude, that models can catch and reproduce the most dominant low-frequency water level variabilities in the Arctic Ocean. Nevertheless, there is need for improvements in terms of seasonal independent analyses and an increased spatio-temporal resolution enabling for example a direct point-wise comparison.

Recent developments in numerical modeling focused on so called unstructured-mesh representations. According to Wang et al. (2014) unstructured ocean model grids local refinements in regions with complex and highly dynamic circulation patterns (e.g. Fram Strait). They allow for multi-resolution analyses of climate relevant variables in specific areas of interest while keeping a coarse spatial representation at other regions on Earth (e.g. Wang et al. (2014), Zhang and Baptista (2008)). One of these models is the Finite Element Sea-ice Ocean Model (FESOM, Wang et al. (2014)). It includes beside the ocean variables (sea surface height, temperature, ocean currents and salinity) a sea-ice component mapping the major ice drift pathways.



Furthermore Wekerle et al. (2017) described a FESOM configuration enabling studies in the Fram Strait and Greenland Sea region on a daily temporal resolution and a spatial refined 1 km mesh, resulting in an eddy-resolving ocean simulation.

In the present study, high-frequency DOT estimates of ESA's Envisat as well as water level outputs of FESOM are used for a direct comparison in order to analyze spatio-temporal correspondence and discrepancies. The investigation aims at exploring capabilities for a combination and exploiting the advantages of both quantities. In particular, it is evaluated if the model outputs can bridge periods when altimetry fails (e.g. due to sea-ice coverage). In the present study, the altimetry database consists of profiled 20Hz DOT snapshots that were preprocessed using the classification presented by Müller et al. (2017). The comparison is conducted in the Greenland Sea and the Fram Strait, covering the East Greenland and the West Spitsbergen Current. The present paper is structured in four main sections. First, the study area and the applied datasets and their pre-processing are introduced, followed by Section 3 describing the comparison methods and displaying the obtained results. The last two sections discuss the results and recapitulate the key aspects.

2 Study area and datasets

This section provides an overview of the study area, the used model, and the observational database. Furthermore, more detailed information on the data pre-processing is given.

2.1 The Greenland Sea and Fram Strait

The study area covers the Greenland Sea and the Fram Strait, as depicted in Figure 1. Moreover, the study area is limited to -30° W to 30° E and 72° N to 82° N. The investigation region constitutes the northern part of the Nordic Seas, which connects the North Atlantic with the Arctic Ocean. The bathymetry is complex in this region: the deep Fram Strait (with depths up to 5.600 m at the Molloy Hole) lies between the wide Northeast Greenland continental shelf and the Svalbard archipelago, with the deep Greenland Sea to the south. Seamounts, ridges and steep slopes affect the ocean circulation.

The northern Nordic Seas are characterized by contrasting water masses. Warm and salty waters of Atlantic origin are carried northward by the Norwegian Atlantic Current (e.g. Orvik and Niiler, 2002). After a bifurcation at Barents Sea Opening, the remaining current that continues northward is termed the West Spitsbergen Current (WSC, e.g. Beszczynska-Möller et al., 2012; von Appen et al., 2016). A fraction of the Atlantic Water carried by the WSC recirculates in the Fram Strait at around 79° N and continues to flow southward, forming the Return Atlantic Water (RAW), whereas the remaining part enters the Arctic Ocean via the Svalbard and Yermak branches (SB and YB). Along the Greenland continental shelf break, the East Greenland Current (EGC, e.g. de Steur et al., 2009) carries cold and fresh Polar Water as well as RAW southward.

Sea ice is exported with the Transpolar Drift out of the Arctic through the Fram Strait. The sea ice export occurs at the western side of the strait, which is thus ice-covered year-round. The eastern part of the Fram Strait is ice-free year-round due to the presence of warm Atlantic water. Around 10% of the Arctic sea ice area is exported through the Fram Strait annually, an order of magnitude larger than the export through other Arctic gateways (Smedsrud et al., 2017).

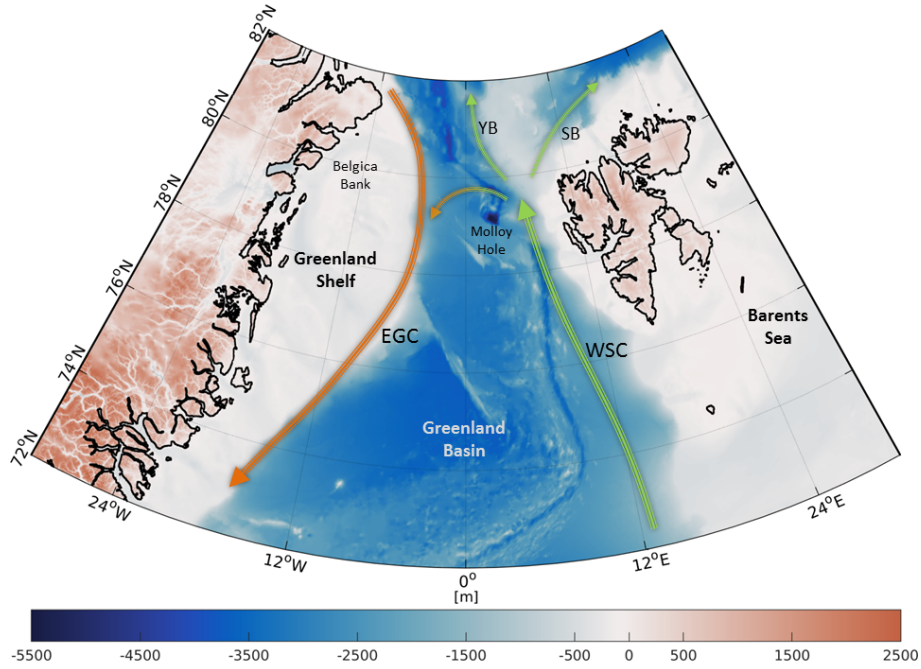


Figure 1. Bathymetry of the Greenland Sea, Fram Strait area based on RTopo2 topography model (Schaffer et al. (2016)). Arrows display major current systems (East Greenland Current, EGC; West Spitsbergen Current, WSC; Yermak Branch, YB and Svalbard Branch, SB). Light green arrows indicate inflowing Atlantic Water; orange represents Returning Atlantic Water.

2.2 Model basis: Finite Element Sea-ice Ocean Model (FESOM)

In this study we use daily mean water level output from the Finite Element Sea-ice Ocean Model (FESOM) version 1.4 (Wang et al., 2014; Danilov et al., 2015). FESOM is an ocean-sea ice model which solves the hydrostatic primitive equations in the Boussinesq approximation. The sea ice component applies the elastic-viscous-plastic rheology (Hunke and Dukowicz, 2001) and thermodynamics following Parkinson and Washington (1979). The finite element method is used to discretize the governing equations, applying unstructured triangular meshes in the horizontal and z-levels in the vertical. Water level heights (in the model labeled as sea surface height) η are computed from the following equation:

$$\partial_t \eta + \nabla \cdot \int_{z=-H}^{z=\eta} \mathbf{u} dz = 0, \quad (1)$$

where $\mathbf{u} \equiv (u, v)$ is the velocity vector and H is the water depth. Water elevations are relative to a geopotential surface and therefore comparable to an altimetry derived dynamic ocean topography (Androsov et al., 2018). The upper limit in the integration is set to zero, which corresponds to a linear free-surface approximation. This implies that the ocean volume does not change with time in the model. To account for surface freshwater fluxes (precipitation, evaporation, river runoff, salinity



changes due to sea ice melting and freezing), a virtual salt flux is introduced (see e.g., Wang et al. (2014)). The model does not take into account sea level pressure and tidal changes.

The global FESOM configuration used here was optimised for the Fram Strait, applying a mesh resolution of 1 km in the area 76°N-82.5°N/20°W-20°E and 4.5 km in the Nordic Seas and Arctic Ocean (Wekerle et al., 2017). In the vertical, 47 z-levels are used, with a thickness of 10 m in the top 100 m and coarser vertical resolution with depth. The model bathymetry was taken from RTopo2 (Schaffer et al., 2016). For the comparison, only the surface information are used (i.e., $z = 0$).

The model is forced by atmospheric reanalysis data COREv.2 (Large and Yeager, 2008), and interannual monthly river runoff is taken from Dai et al. (2009). A sea surface salinity restoring to the PHC 3.0 climatology (Steele et al., 2001) is applied with a restoring velocity of 50 m per 300 days. The simulation covers the time period 2000 until 2009, and daily model output was saved. A comparison with observational data (e.g. moorings) revealed that the model in simulating the circulation structure, hydrography and eddy kinetic energy in the Fram Strait (Wekerle et al., 2017).

2.3 Observational basis: Radar Altimetry Data

In the present study high-frequency radar altimetry data of the ESA satellite Envisat is used. The altimeter emits radar signals in *Ku*-band with a footprint (i.e. circular area on the ground illuminated by the radar) of approximately 10 km diameter (Connor et al., 2009). Envisat belongs to the pulse-limited altimetry missions and provides observations characterized by a spatial along-track resolution of circa 372 m (18Hz). The mission was placed in orbit in 2002 and provided altimetry data until end of March 2012. This study uses high-frequency waveform data that are extracted from the official Sensor Geophysical Data Records (SGDR) version 2.1 provided by ESA. Data measured during the nominal mission period (05/2002-10/2010) is organized into 35 days repeat cycles including a fixed relative orbit number (i.e. pass, from pole to pole) of 1002 passes per cycle (ESA, 2011). Considering the temporal availability of FESOM and reliable observations of Envisat, SGDR data of a period covering seven complete years (2003-2009) is used. Before using the Envisat altimetry observations, a classification is performed to eliminate sea-ice contaminated measurements. Sea surface heights (SSH) are calculated by applying the ALES+ retracking algorithm (Passaro et al., 2018) and geophysical corrections. Unrealistic or bad height measurements are excluded by performing an outlier detection based on sea level anomalies. Finally, a transformation to physical heights (dynamic ocean topography, DOT) is processed by subtracting geoid heights from SSH. Following subsections describe more detailed the individual pre-processing steps.

2.3.1 Sea-ice/Water Discrimination

Most of the Arctic regions are affected by a seasonal sea-ice cover, which can prevent a reliable estimation of sea surface heights due to a direct impact on the reflected radar pulses. In order to overcome this difficulty and to allow for a SSH comparison with FESOM, a classification is performed to detect small open water gaps (e.g. leads, polynyas) within the sea-ice covered area. For this purpose an unsupervised classification approach (i.e without the use of any training data) based only on radar waveforms and derived parameters is applied. Briefly summarized, the unsupervised classification approach, described by Müller et al. (2017), groups an unassigned subset of altimetry radar waveforms into a predefined number of



classes by applying a partitional cluster algorithm (i.e. K-medoids) in order to establish a reference waveform model to indicate different waveform and surface characteristics. In the following step, the generated waveform model acts as kind of assignment map for the remaining waveforms, which are allocated to the particular classes using a simple K-nearest-neighbor classifier. Further information and explanations can be found in Müller et al. (2017). The open water (leads, polynyas and open ocean) observations are used for all following processing steps. Measurements classified as ice are removed from the dataset. However, it has to be noted that some mis-classifications, e.g. due to the presence of fast ice, can still remain in the observation dataset (Müller et al., 2017).

2.3.2 Sea Surface Height Estimation

SSH are obtained by subtracting the measured range between satellite and water surface (including geophysical corrections) from the orbital altitude (i.e. ellipsoid height) of the satellite's center of mass. The range can be calculated by fitting a waveform model (e.g. Brown (1977) or Hayne (1980)) to the individual radar returning signals. More information regarding retracking strategies can be found for example in Vignudelli et al. (2011). Several retracking algorithms have been developed and optimized for special applications, surface conditions or study regions (e.g. open ocean, sea-ice or inland water bodies). According to Serreze and Barry (2014) the Greenland Sea is characterized by rapid changing environmental conditions making it difficult to use just one retracking algorithm. However, when combining heights derived with different retrackers, systematic offsets due to different retracker biases will be introduced (Bulczak et al. (2015)). The usage of ALES+ overcomes this problem by adapting a subwaveform application of the classic open ocean functional form to different shapes of the radar signals, including typical peaky signal shape of the returns from small leads and corrupted trailing edges typical of coastal waveforms. Passaro et al. (2018) have developed and tested the algorithm against standard open ocean and lead retrackers and showed improvements in precision and in terms of comparison with a local tide gauge. The algorithm was used to develop and Antarctic products in the framework of the ESA Sea Level Climate Change Initiative (Legeais et al., 2018).

After the retracking, the altimeter ranges are corrected for geophysical and atmospheric effects, using external model data. Wind and wave effects are considered by using the sea state bias estimates of the ALES+ retracking approach. Furthermore radial orbit error corrections, gathered by a multi-mission crossover analysis (Bosch et al., 2014), are included to eliminate offsets between the various satellite missions. Table 1 lists all corrections used within the present investigation.

To remove erroneous and unreliable sea surface height observations from the dataset an outlier rejection is performed by applying a fixed threshold criteria. The SSH observations are compared to a long-temporal Mean Sea Surface (MSS), and sea level anomalies (SLA) are build. The conversion is done by removing the DTU15MSS developed by Andersen and Knudsen (2009) from the along-track sea surface heights. Without being too restrictive within the sea-ice zone with higher noise level than in open ocean, a threshold of $\pm 2m$ is introduced. This rejects 1.54% of the high-frequency measurements of Envisat. After removing outliers the revised dataset is retransformed to sea surface heights by re-adding the MSS.



Table 1. Geophysical and empirical corrections applied in the study

| Corrections | Sources | References |
|-----------------------------|---|--|
| Ionosphere | NOAA Ionosphere Climatology 2009 (NIC09) | Scharroo and Smith (2010) |
| Wet troposphere | ECMWF (2.5° × 2.0°) for Vienna Mapping Functions (VMF1) | Boehm et al. (2009) |
| Dry troposphere | ECMWF (2.5° × 2.0°) for Vienna Mapping Functions (VMF1) | Boehm et al. (2009) |
| Inverse barometric pressure | Dynamic Atmospheric Correction (MOG2D)HF | Collecte Localisation Satellites (CLS) |
| Ocean tides | Global Empirical Ocean Tide model (EOT11a) | Savcenko et al. (2012) |
| Pole tides | from Envisat SGDR v2.1 | Wahr (1985) |
| Solid Earth tides | from Envisat SGDR v2.1 | Cartwright and Edden (1973) |
| Radial errors | multi-mission cross-calibration (MMXO) Version: 15 | Bosch et al. (2014) |
| Sea State Bias | ALES+ Sea State Bias correction | Passaro et al. (2018) |

2.3.3 Dynamic Ocean Topography Estimation

After obtaining sea surface heights the transition to physical heights is performed with respect to an underlying geoid model (i.e. the computation of DOT). In the present investigation the high resolved Optimal Geoid Model for Modeling Ocean Circulation (OGMOC), developed up to harmonic degree of 2190, corresponding to a spatial resolution of nearly 9.13 km, is applied. More details regarding to the constituents and processing strategy of the geoid can be found in Fecher and Gruber (2018).

To minimize noise within the high-frequency altimetry database and to be more consistent with the spatial resolution of the geoid, the corrected along-track SSH observations get low-pass filtered by applying a moving average using a rectangle kernel adapted to the spatial resolution of the used geoid. Areas with sparse availability of along-track observations (e.g. leads, polynyas), less than the window size are not considered in the filtering process and remain unfiltered in the dataset. The DOT is derived by interpolating the geoid heights to the altimetry locations and subtracting them from the SSH observations.

3 Methods and Results

The preprocessed ocean heights from altimetry and FESOM are compared with each other to identify similarities and discrepancies, and to explore the possibility for a combination. Therefore, in a first step, both datasets are analyzed and examined regarding their temporal and spatial characteristics. The datasets are investigated in terms of constant offsets, seasonal occurring patterns (e.g. annual sea level variability) and the residual sea level variations.

The FESOM data is provided on daily unstructured grids with local refinements in the central Greenland Sea and the Fram Strait. In contrast, the altimetry observations are sampled along-track and characterized by a high-spatial resolution with irregular data gaps due to sea ice coverage. Figure 2 displays the inhomogeneous distributed FESOM nodes showing a maximum resolution of about 1 km. Moreover, three representative days of altimetry along-track data are shown with different behav-

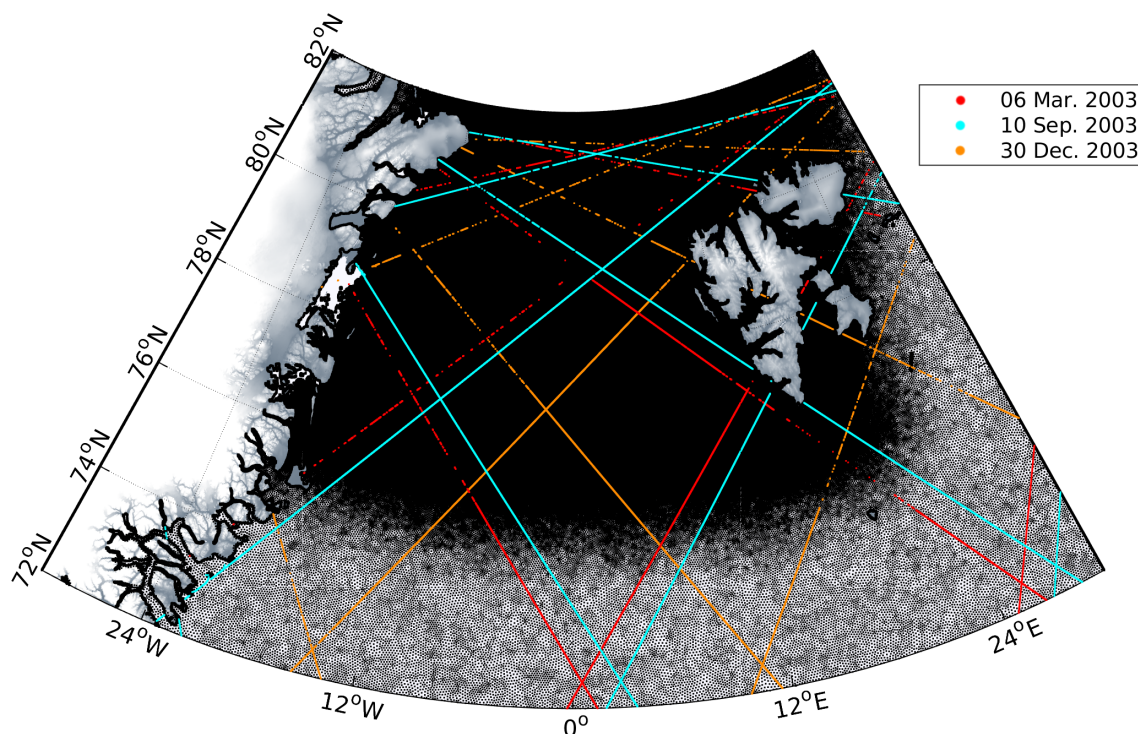


Figure 2. Locations of selected altimetry observations in winter and summer time. The small black dots indicate the unstructured FESOM grid nodes migrating at higher latitudes to a apparently closed black background.

ior in observation availability depending on the season and the presence of sea-ice. During the sea-ice maximum in March (Kvingedal, 2013) most of the altimetry data close to the Greenland coast is missing due to a semi closed sea-ice cover. In contrast, in the summer season the tracks show less data gaps.

In order to allow a direct and point-wise comparison of both datasets, a re-sampling of at least one of them is necessary. Since the FESOM data exhibits a significant higher spatial and an uniform temporal resolution, it will be interpolated to the times and locations of the altimetry observations. This prevents an unnecessary smoothing of the altimetry data.

3.1 Assessment of the Annual Cycle

It can be expected that the annual sea level variability as the dominant signal is contained in both data sets (e.g. Bulczak et al. (2015)). The present analysis performs a comparison of the annual and the remaining temporal signal components within the investigation period by fitting harmonic functions to both datasets.

In a first step, daily height averages for the entire region are computed. Figure 3 shows the temporal evolution of the daily means within the investigation period for both datasets. An obvious offset of about 41 cm between the datasets caused by different underlying height references (geoid vs. bathymetry) is clearly visible. Furthermore, a linear trend or another long-term systematic behavior is not detectable, probably due to the short period of only seven years. However, the altimetry derived

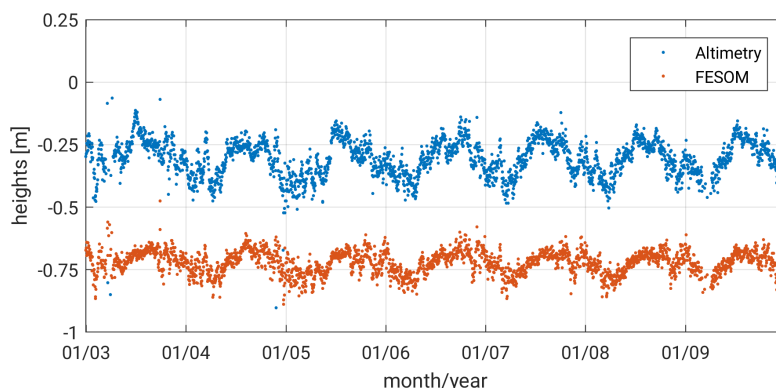


Figure 3. Temporal evolution of daily means of altimetry derived DOT observations (blue) and FESOM SSH outputs (interpolated to the locations of altimetry measurements, red) within the investigation period and study area (see Section 2).

daily averaged DOT shows larger variations and a standard deviation of 9.0 cm. In contrast, the modeled data is characterized by a smoother behavior and a smaller standard deviation of 4.7 cm. These numbers include a clear seasonal cycle, which is also clearly visible in Fig.3.

In order to examine both datasets concerning their annual period, the daily means are analyzed by a Fourier analysis (e.g. Stade (2005)). Therefore, both time series are centered at zero by reducing their constant offsets before the Fourier coefficients are obtained by applying a least-square estimation.

Figure 4a displays the amplitude spectrum of the interpolated FESOM and profiled altimetry daily means between 2003 and 2009. The modeled data is characterized by weaker amplitudes. The annual period constitutes the most dominant long-period signal. In case of altimetry, the annual amplitude represents 6.9 cm and in case of FESOM, 3.9 cm of the sea level variability. Other frequencies can not be physical explained and thus are not further investigated in the present study. Especially, the semi-annual signal is very small (1.5 cm) and shows no significant impact on both datasets. The remaining amplitudes are smaller than 1.5 cm in case of altimetry (1.0 cm, FESOM).

However, an amplitude of almost 2 cm is detectable for a period of three days, which cannot be assigned to ocean or sea-ice related dynamics. This is an artifact owing to the irregular data sampling. In order to investigate these effects in more details, the full FESOM grid data is used for the frequency analysis. Figure 4b shows the amplitude spectrum and the estimated periods for the daily profiled FESOM DOT (red) and the original FESOM DOT (black). It can be clearly observed that the 3 days period is not confirmed by the original dataset. However, all other dominant periods are caught by both datasets. The obtained amplitudes show good agreement in all periods. However, higher discrepancies can be found in the short periodic domain, which can be addressed to a more unreliable coefficient estimation due to more input information.

As mentioned earlier the annual signal represents the most dominant signal in both datasets. Introducing the obtained annual Fourier coefficients to a harmonic fitting, the temporal evolution and the phasing can be shown (see Figure 5). Beside

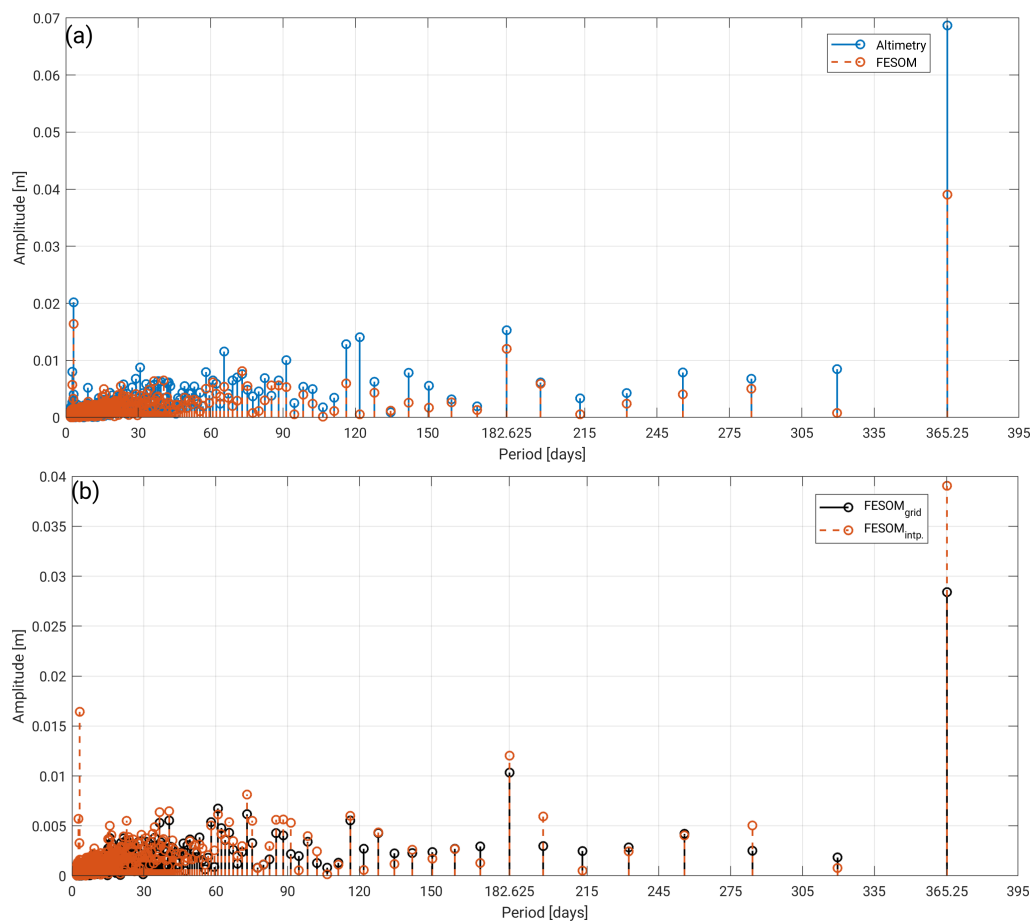


Figure 4. Fourier analysis amplitude spectrum of to altimetry locations interpolated FESOM data (red) with (a) altimetry derived DOT along-track observations (blue) and (b) original FESOM (black) within the investigation area and time from 2003 - 2009 (see Sect. 2).

differences in the annual amplitudes, a phase shift of about 29 days is recognizable between the two signals. The maximum is reached at day of year (DOY) 230 (18-Aug.) for altimetry and in case of FESOM at DOY 259 (16-Sept.).

However, it is obvious that one single harmonic function cannot represent the full complexity of the DOT variations in the entire Greenland Sea. A detailed analysis of the annual signal considering different bathymetric features (e.g. shelf- or deep sea areas) brings the opportunity to estimate region dependent annual amplitudes and phases. This is presented in the following section.

3.2 Spatio-temporal pattern analysis

In order to analyze regional dependent differences, the profiled altimetry data is monthly averaged and arranged into along-track bins of 7.5 km length. The bin structure follows the nominal ground track pattern of Envisat. Enabling long-term analyses,

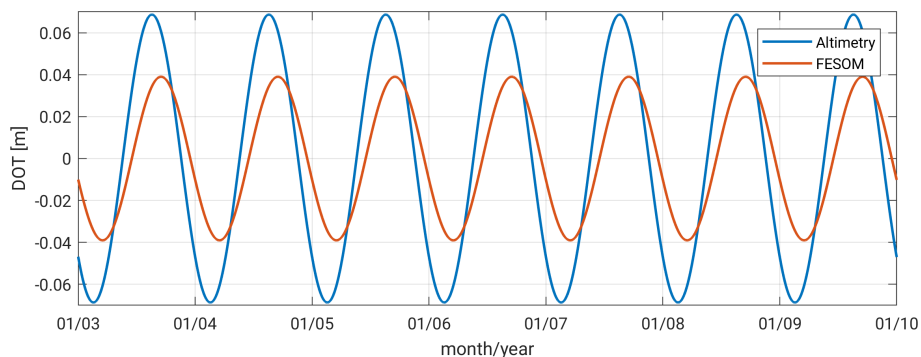


Figure 5. Annual cycles of DOT from along-track altimetry (blue) observations and FESOM (red) simulation within investigation time and area (see Sect. 2).

only satellite passes are admitted showing an availability of at least 64 repeat cycles, which corresponds to 96% of the data in the evaluation period. Data gaps or missing bins are possible due to sea-ice contamination or failing observations. For FESOM, daily data from the closest grid node are assigned to each bin. Thus, this dataset exhibits the same spatial, but a better temporal resolution, allowing for a more precise amplitude estimation.

5 Figure 6 displays for each bin the estimated annual DOT variations within 2003 - 2009. The amplitudes of both datasets show a similar pattern with smaller values along the major current systems (EGC and WSC) and larger values along the Greenland and Svalbard Coasts and in the area around the Molloy Hole. In general, the altimetry derived amplitudes are larger than the model amplitudes. In the Greenland Basin, a 2-3 times stronger representation of the annual amplitudes can be observed. Here, the mean altimetry amplitude reaches 6.3 cm. In the southern and eastern parts of the shelf regions, the altimetry amplitudes
10 are smaller than the model amplitudes.

The maximum amplitudes in the Greenland Basin appear during August and September and show a mostly homogeneous distribution in both datasets. In ice-free regions both datasets show good agreement (also in comparison with results of Volkov and Pujol (2012) and Mork and Øystein Skagseth (2013)). However, in ice covered shelf regions, the central Fram Strait and close to calving glaciers, the derived amplitudes differ up to 8 cm. The altimetry estimated annual maximum on the Greenland
15 Shelf occurs in November, which is confirmed by FESOM. Nevertheless, obvious phase differences between FESOM and altimetry can be found eastwards of Spitsbergen, where the observed annual maximum occurs in the early spring months, in contrast to FESOM displaying a maximum in autumn. This can perhaps be caused by sea-ice interferences or strong ocean variabilities.

In order to account for different hydrological (e.g. glacier melt, water mass changes), atmospheric (e.g. winds, solar radiation) and oceanographic effects (e.g. ocean currents) in the study area, the region is subdivided into three main subareas: the deep-basin (Greenland Basin, <-450 m) and two shelf regions (Greenland Shelf, Barents Sea). Table 2 provides outlier removed (3-sigma criterion) mean amplitudes and DOYs of the maximum amplitude for the three sub-regions, as well as their annual variabilities. FESOM shows similar amplitudes for all three areas, whereas altimetry exhibits smaller mean amplitudes for the
20



Barents Sea than for the two other regions, where the mean amplitudes are about twice the amplitudes of FESOM. The phase shows good consistency between altimetry and FESOM on the Greenland Shelf, but discrepancies of circa 34.25 days in the Greenland Basin and 19.5 days in the Barents Sea. A discussion of the differences is provided in Section 4.

3.3 Residual Analysis

5 In order to analyze residual differences, both datasets are reduced by their regional estimated annual signal and constant offsets as given in Table 2. Figure 7 shows monthly averaged along-track residual DOT for altimetry and FESOM for the three study regions. In all areas, a high correlation between the datasets is visible. For the Greenland Basin and the Barents Sea, almost no systematic effects are detectable, whereas, the altimetry time series for the Greenland Shelf exhibits multi-annual anomalies that are less pronounced in the FESOM time series, which only shows a small, insignificant trend behavior. However, the
 10 investigation period is too short to allow for a reliable interpretations of the underlying effects.

Figure 8 shows the geographical distribution of the mean residual signals and weighted average of standard deviation per bin. Both datasets display similar spatial patterns. However, obvious differences can be seen in some areas, e.g., the central Fram Strait and the transition areas between deep-basin and shelf regions. Comparing the variability of the residuals, the altimetry derived DOT shows in general higher values and an enhanced variations in the ice-covered shelf areas, contrary to FESOM
 15 displaying more variability in regions affected by ocean currents.

Figure 9 shows the differences between the averaged residual DOT of altimetry and FESOM (left) as well as their correlation per bin (right). The largest differences occur in the northern Greenland Shelf and Fram Strait, whereas less sea-ice affected areas (e.g. Greenland Basin, Barents Sea) including the current and eddy regions (e.g. WSC) show good agreement. The correlations are mainly positive, with values above 0.5 for 21% of the bins. High positive correlations are displayed in the deep-basin parts
 20 of the study area. Smaller positive correlations can be found in regions with strong bathymetric gradients and in northern areas of the major ocean currents (e.g. WSC, EGC).

Table 2. Offset, averaged annual amplitude (Amp) and day of year (DOY) / month of maximum amplitude with variability (Var) in three sub-regions

| Area | Source | Offset (Var) [m] | Amp (Var) [m] | DOY/Month (Var) |
|-----------------|-----------|------------------|---------------|----------------------|
| Greenland Basin | Altimetry | -0.301 (0.131) | 0.063 (0.023) | 232.75/Aug. (33.61) |
| | FESOM | -0.744 (0.086) | 0.030 (0.009) | 267/Sept. (29.24) |
| Greenland Shelf | Altimetry | +0.054 (0.099) | 0.057 (0.038) | 314.75/Nov. (112.86) |
| | FESOM | -0.537 (0.054) | 0.038 (0.013) | 312.25/Nov. (21.38) |
| Barents Sea | Altimetry | -0.180 (0.043) | 0.040 (0.018) | 284.25/Oct. (102.42) |
| | FESOM | -0.667 (0.020) | 0.038 (0.010) | 303.75/Oct. (13.04) |

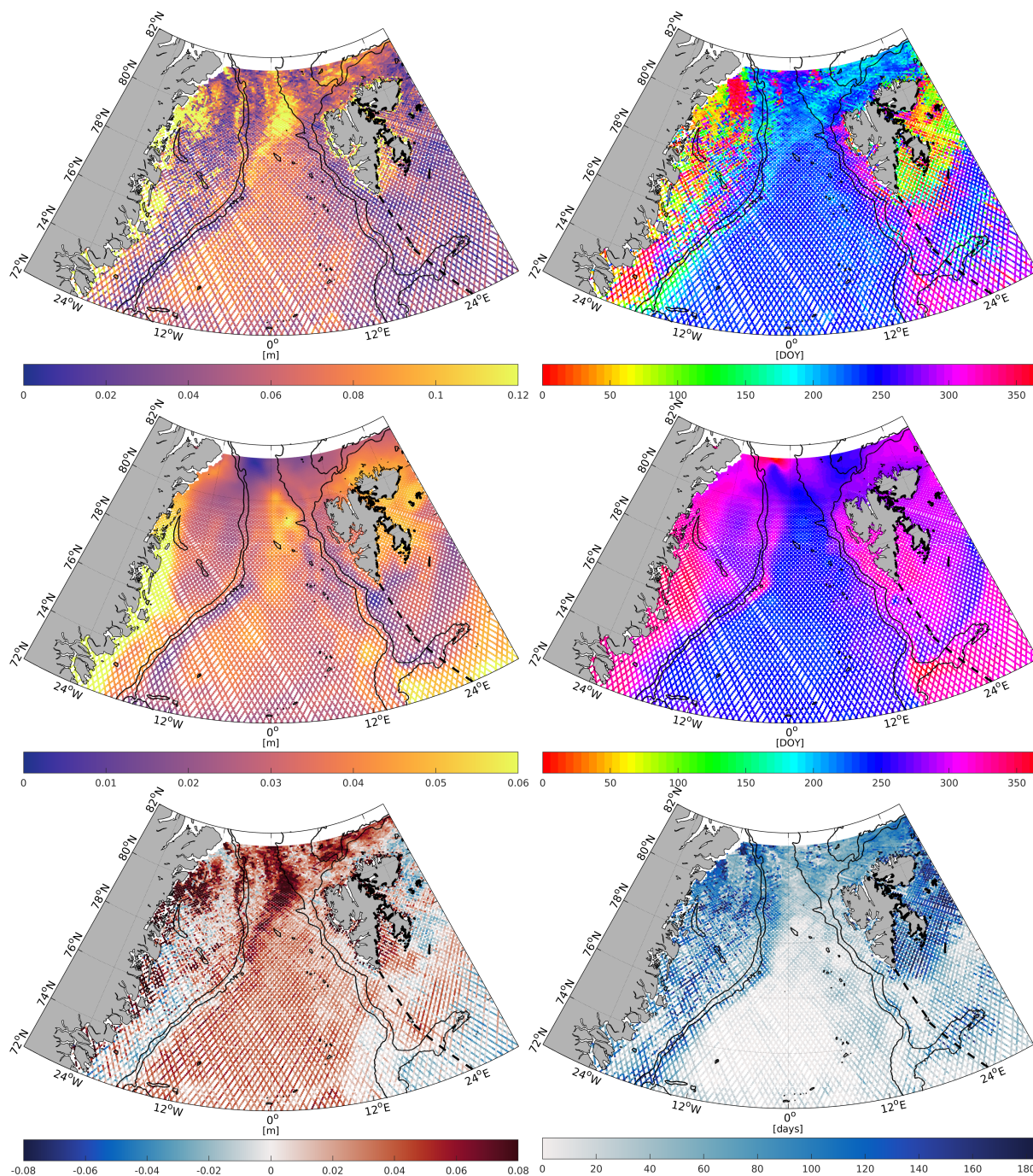


Figure 6. Mean annual amplitudes (left) and day of year (DOY) of annual maximum (right) per bin for altimetry (top) and FESOM (middle) DOT heights. Bottom row displays amplitude and phase differences of Altimetry minus FESOM. RTopo2 bathymetric contours (black) indicate shelf (-450 m) and the basin (-1500 m) regions. Dashed line highlight the Barents Sea boundary (IHO, International Hydrographic Organization (1953)). Note the different scales of the amplitude color bars.

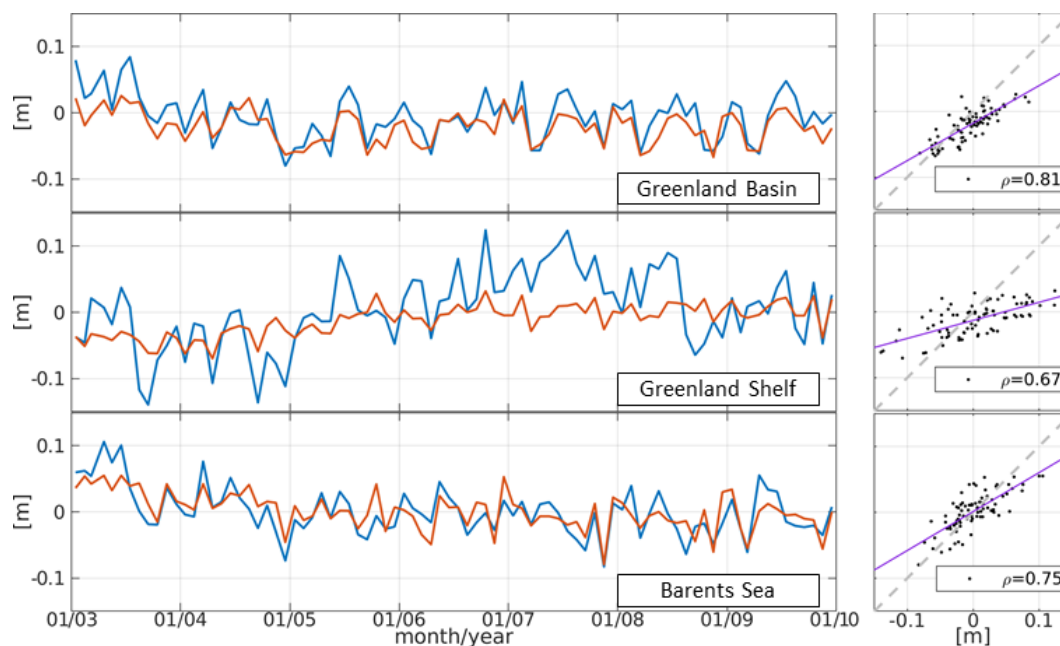


Figure 7. Monthly time series of averaged residual heights from altimetry (blue) and FESOM (red). Offsets and annual signals were removed for each region. Additionally scatter plots and correlation (ρ) are displayed. Regression and bisectrix lines are shown in purple and gray dashed.

Remarkable elevation differences occur between 80° N and 82° N. These patterns originate from the altimetry DOT and yield up to 0.4 m. They show a constant behavior within the entire investigation period, which cannot be addressed to seasonal ocean phenomena. Instead, these artifacts are due to insufficient sampling of the underlying geoid model at the polar latitudes (e.g. Kwok and Morison (2015), Farrell et al. (2012)). More discussion related to the geoid can be found in the next section.

5 4 Discussion

The comparison of the altimetry derived and simulated DOT shows good accordance in terms of highly correlated regional time series and small residual heights. Predominately positive correlations between both datasets can be found in ice-free areas (e.g. Greenland Basin) and in regions affected by ocean currents. FESOM and altimetry display a very similar frequency behavior of the most dominant periodic DOT variability. In comparison with previous studies the along-track altimetry DOT agrees
 10 concerning annual amplitudes and phases obtained by Volkov and Pujol (2012) and Mork and Øystein Skagseth (2013).

However, the analysis also reveals some systematic discrepancies. These can be explained by three different error sources: They partly originate from modeling errors of FESOM, partly from measurement uncertainties of altimetry, and partly from errors of the geoid used for computing the altimetry DOT. These points will be discussed in more detail in the following paragraphs.

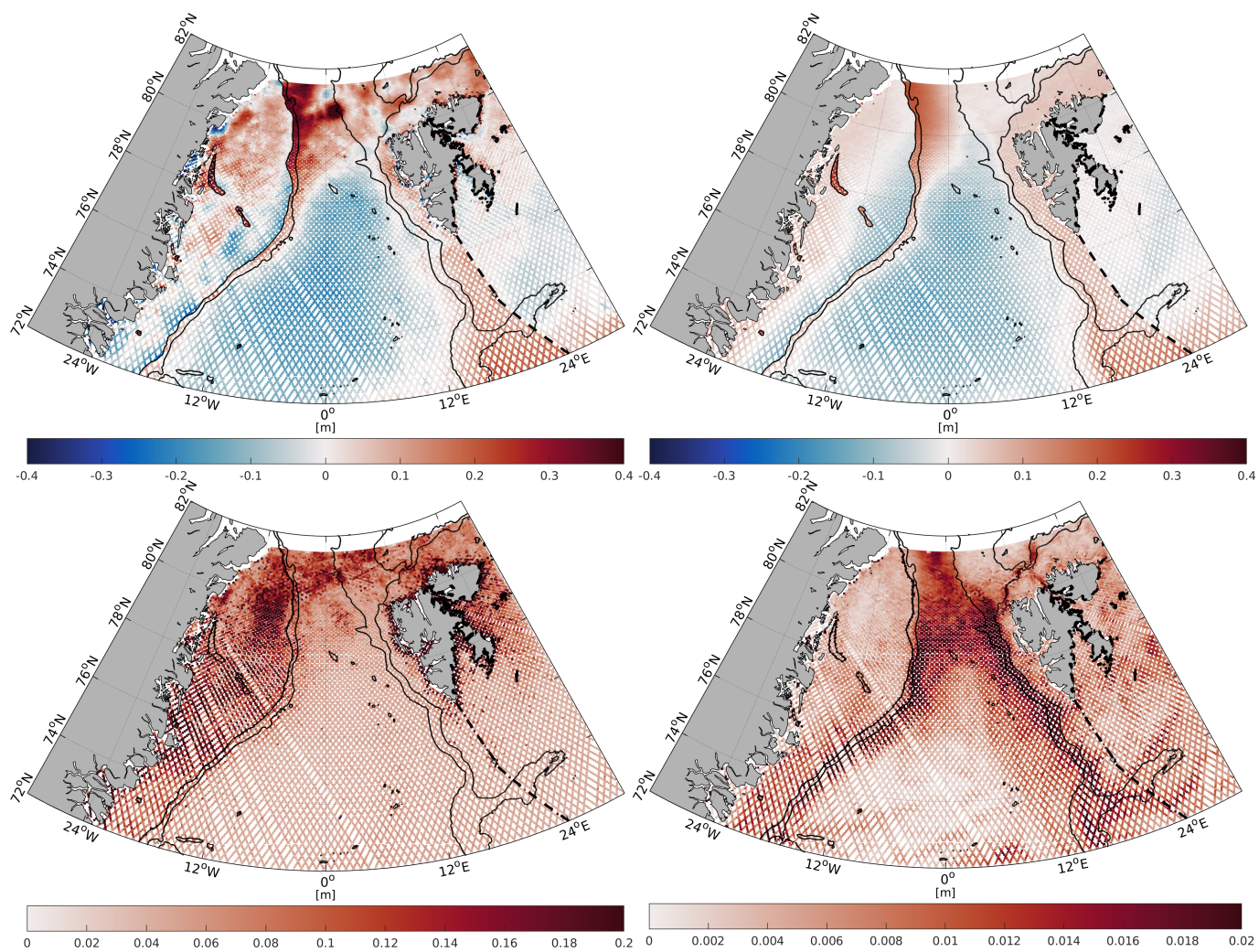


Figure 8. Weighted mean residual DOT (top) and weighted mean of standard deviation (bottom) for each bin from altimetry (left) and FESOM (right) within 2003 -2009. Note the different scales of standard deviation color bars.

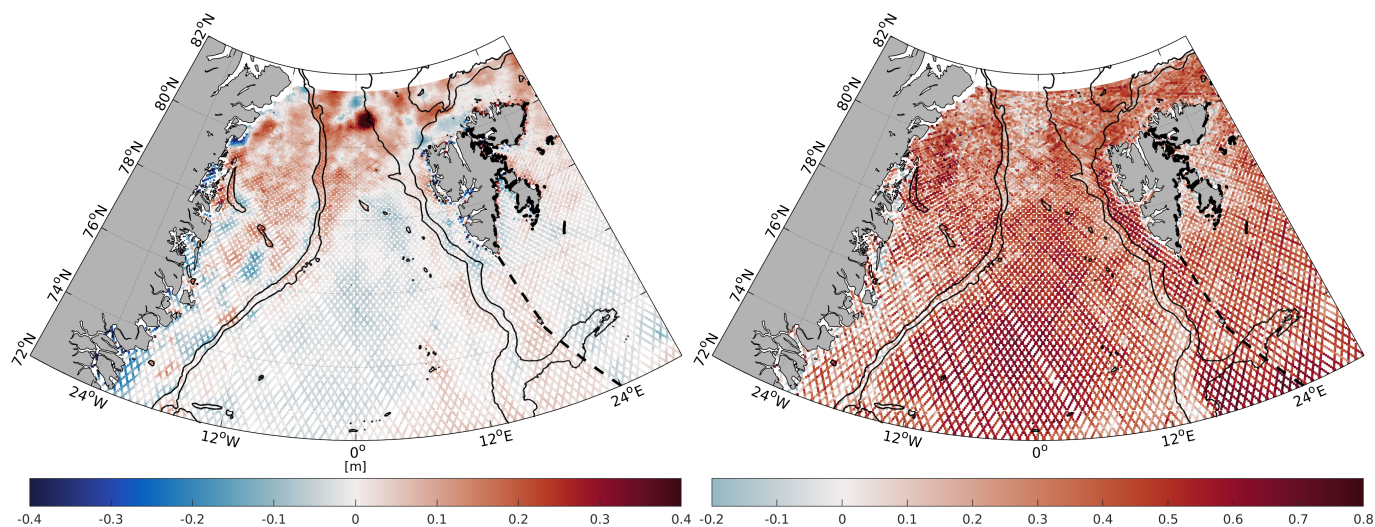


Figure 9. Differences (left) and correlations (right) between altimetry and FESOM binned along-track residual DOT within the investigation period.

FESOM is affected by synthetic smoothing, due to the added numerical diffusion part, stabilizing the model runs and preventing the simulated DOT from uncontrolled variabilities. Moreover, in the present investigation the FESOM run does not include the latest glacier runoff model, which causes further irregularities close to North-East Greenland's coast. Another reason causing smoothing effect can be found in a too strong adjusted sea-ice friction coefficient of the model, damping DOT variabilities in sea-ice affected regions. The model applies strictly the hydrostatic equations, which act as kind of assumption to the real sea state. Furthermore, it ignores tidal and barometric effects and is restricted to steric and ocean mass movements. Even the missing atmospheric sea level pressure causes temporal shifts of the maximum annual signal in the Greenland Basin. An incomplete representation of the sea level, particularly the ocean bottom pressure, is a reason for significant smaller annual amplitudes than in the altimetry observations.

For satellite altimetry, the polar oceans are a challenging region, especially, when sea-ice is present. Even with the applications of a dedicated waveform classification and a special retracking, as performed here, DOT estimates in coastal and sea-ice areas are significant noisier than in open ocean. Moreover, the applied range corrections can be biased by the Arctic Ocean conditions leading to more unreliable range estimations in ice covered shelf regions. Thus, in these regions, small-scale structures are not thoroughly reliable.

This study is based on data from Envisat whose repeat cycle is known to cause severe alias effects of 365 days for the tidal constituents K1 and P1 (Volkov and Pujol (2012) and Padman et al. (2018)). Thus, errors in K1 and P1 of the applied ocean tide model may impact the estimated annual variation of the altimetry based DOT. Passaro et al. (2015) showed that the effect can reach up to 1-3 cm. For this study, the EOT11a ocean tide model (Savcenko et al. (2012)) is used. Even if that model is proven to be among the best models in the Arctic Ocean (see Stammer et al. (2014)) the differences between FESOM and altimetry in the bin-wise estimated annual amplitudes could be partially attributed to this aliasing effect. However, the analysis presented



in section 3.1, which is based on averaged Envisat data, also shows a discrepancy of more than 1 cm between FESOM and altimetry amplitudes. Thus, most part of this difference will be due to the smoothing effect of FESOM.

Beside simulated and observational data irregularities, stationary artifacts caused by geoid inaccuracies can be clearly identified in the northern Fram Strait region. Following Kwok and Morison (2015) these synthetic looking elevations in the altimetry derived DOT can be addressed to a combination of geoid residuals and oceanographic features, which are very challenging to separate from each other. A significant problem can be seen in the specific components of the geoid models. The higher spherical harmonics (degrees 720-2190), describing shorter wavelength patterns (10 km - 30 km), are based on selective in-situ and satellite altimetry gravity observations, which can be contaminated by sea-ice or featured by sparse availability. Within this study, one of the newest geoid models is used, which has been developed for ocean circulation studies and has been optimized to avoid striations and orange skin like features. Nevertheless, it seems to contain remaining artificial structures in the study area. According to Fecher and Gruber (2018) the higher spherical harmonics are covered by EIGEN-6C4 geoid model (Förste et al., 2004), which does not include current satellite altimetry data. However, mid spherical harmonic degrees, corresponding to 30 km - 100 km spatial wavelength, are represented by XGM2016 (Pail et al., 2018) including latest altimetry marine gravity fields. Hence, a better representation of short wavelength patterns can only be reached by introducing latest and updated altimetry data, supported by in-situ measurements to the geoid computations. Similar effects are also visible when using alternative geoid models (Skourup et al., 2017).

5 Conclusions and Outlook

In the present paper, high-frequency altimetry derived DOT are compared with water elevations of FESOM in order to identify similarities and discrepancies as well as respective benefits. Both datasets are characterized by different limitations, which prevent a perfect representation of the dynamic topography in polar regions just based on only one approach. The present investigation demonstrates that model simulations and observations are both needed to understand the complexity of ocean processes in the polar latitudes, especially in the Arctic Ocean.

The present paper indicates basic accordance between a numerically simulated and an empirical estimated representation of the DOT in the Greenland Sea in terms of annual variability and spatial behavior. However, inconsistencies due to the higher noise level of the observations, especially in sea-ice areas and the enhanced smoothing of the model are demonstrated. For example, an offset of about half a meter exists between the two datasets since the datum of FESOM is not defined with respect to a standard reference frame (Androsov et al., 2018). Moreover, the annual sea level variability observed by the two datasets differs by a few centimeters. The residual heights show a similar pattern, high temporal correlations and only small differences, which are mainly related to sea-ice coverage and geoid artifacts.

The result presented in this paper indicate that further improvements can be made for both datasets: The altimetry-derived DOT still needs a better or more restrictive handling of sea-ice observations as well as a more reliable Arctic geoid. FESOM should be extended by barometric effects for example the so-called Graetbatch correction (Greatbatch, 1994) and a better glacier runoff model. However, even if these points will be improved, the principle limitations of observations (measurement



noise and data gaps in regions with closed sea ice coverage) and models (absolute height level) will persist. Thus, it seems reasonable to exploit the advantages of both datasets by a combination of model and observations. In such an approach, the absolute level as well as the annual variability of altimetry should be preserved and the continuous spatial representation of the model shall be used to bridge regions influenced by sea-ice coverage and to get rid of unreliable high-latitude geoid artifacts.

5 This will allow for an optimized determination of the Arctic DOT and the associated surface currents. Concerning the current availability of altimetry derived DOT estimations it is possible to establish a more than 25 years covering combination of simulated and observation based DOT representation, enabling climate relevant conclusions.

Acknowledgements. The authors thank ESA for operating Envisat as well supplying the SGDR v2.1 dataset. The authors thank the Chair of Astronomical and Physical Geodesy, Technical University of Munich (TUM) for providing the geoid model, OGMOC. This work was mainly supported by the German Research Foundation (DFG) through grants, BO1228/13-1, DE2174/3-1 and in part through grant (OGreen79) as part of the Special Priority Program (SPP)-1889 "Regional Sea Level Change and Society" (SeaLevel). The publication is funded by German Research Foundation (DFG) and the Technical University of Munich (TUM) in the framework of the Open Access Publishing Program.

10

Author contributions. Felix L. Müller developed the comparison methods, conducted the data analysis and wrote the majority of the paper. Claudia Wekerle provided the FESOM data and contributed to the manuscript writing. Denise Dettmering supervised the present study, contributed to the manuscript writing and helped with discussions of the results. Marcello Passaro developed the retracking algorithm and helped with the application and discussion concerning the altimetry dataset. Wolfgang Bosch initiated the study. Florian Seitz supervised the research.

15

Competing interests. The authors declare no conflict interests.



References

- Andersen, O. B. and Knudsen, P.: DNSCO8 mean sea surface and mean dynamic topography models, *Journal of Geophysical Research: Oceans*, 114, <https://doi.org/10.1029/2008JC005179>, c11001, 2009.
- Androsov, A., Nerger, L., Schnur, R., Schröter, J., Albertella, A., Rummel, R., Savcenko, R., Bosch, W., Skachko, S., and Danilov, S.: On the assimilation of absolute geodetic dynamic topography in a global ocean model: impact on the deep ocean state, *Journal of Geodesy*, <https://doi.org/10.1007/s00190-018-1151-1>, 2018.
- Armitage, T. W. K., Bacon, S., Ridout, A. L., Thomas, S. F., Aksenov, Y., and Wingham, D. J.: Arctic sea surface height variability and change from satellite radar altimetry and GRACE, 2003–2014, *Journal of Geophysical Research: Oceans*, 121, 4303–4322, <https://doi.org/10.1002/2015JC011579>, 2016.
- 10 Beszczynska-Möller, A., Fahrbach, E., Schauer, U., and Hansen, E.: Variability in Atlantic water temperature and transport at the entrance to the Arctic Ocean, 1997–2010, *ICES J. Mar. Sci.*, 69, 852–863, <https://doi.org/10.1093/icesjms/fss056>, 2012.
- Boehm, J., Kouba, J., and Schuh, H.: Forecast Vienna Mapping Functions 1 for real-time analysis of space geodetic observations, *Journal of Geodesy*, 83, 397–401, <https://doi.org/10.1007/s00190-008-0216-y>, <https://doi.org/10.1007/s00190-008-0216-y>, 2009.
- Bosch, W., Dettmering, D., and Schwatke, C.: Multi-Mission Cross-Calibration of Satellite Altimeters: Constructing a Long-Term Data Record for Global and Regional Sea Level Change Studies, *Remote Sensing*, 6, 2255–2281, <https://doi.org/10.3390/rs6032255>, 2014.
- 15 Brown, G.: The average impulse response of a rough surface and its applications, *IEEE Transactions on Antennas and Propagation*, 25, 67–74, <https://doi.org/10.1109/TAP.1977.1141536>, 1977.
- Bulczak, A. I., Bacon, S., Naveira Garabato, A. C., Ridout, A., Sonnewald, M. J. P., and Laxon, S. W.: Seasonal variability of sea surface height in the coastal waters and deep basins of the Nordic Seas, *Geophysical Research Letters*, 42, 113–120, <https://doi.org/10.1002/2014GL061796>, [2014GL061796](https://doi.org/10.1002/2014GL061796), 2015.
- 20 Cartwright, D. E. and Edden, A. C.: Corrected Tables of Tidal Harmonics, *Geophysical Journal International*, 33, 253–264, <https://doi.org/10.1111/j.1365-246X.1973.tb03420.x>, 1973.
- Collecte Localisation Satellites (CLS): Dynamic atmospheric Corrections are produced by CLS Space Oceanography Division using the Mog2D model from Legos and distributed by Aviso+, with support from Cnes, AVISO+, <http://www.aviso.altimetry.fr>.
- 25 Connor, L. N., Laxon, S. W., Ridout, A. L., Krabill, W. B., and McAdoo, D. C.: Comparison of Envisat radar and airborne laser altimeter measurements over Arctic sea ice, *Remote Sensing of Environment*, 113, 563–570, <https://doi.org/10.1016/j.rse.2008.10.015>, 2009.
- Dai, A., Qian, T., Trenberth, K. E., and Milliman, J. D.: Changes in Continental Freshwater Discharge from 1948 to 2004, *J. Climate*, 22, 2773–2792, <https://doi.org/10.1175/2008JCLI2592.1>, 2009.
- Danilov, S., Wang, Q., Timmermann, R., Iakovlev, N., Sidorenko, D., Kimmritz, M., Jung, T., and Schröter, J.: Finite-Element Sea Ice Model (FESIM), version 2, *Geosci. Model Dev.*, 8, 1747–1761, <https://doi.org/10.5194/gmd-8-1747-2015>, 2015.
- 30 de Steur, L., Hansen, E., Gerdes, R., Karcher, M., Fahrbach, E., and Holfort, J.: Freshwater fluxes in the East Greenland Current: A decade of observations, *Geophys. Res. Lett.*, 36, <https://doi.org/10.1029/2009GL041278>, 2009.
- ESA: ENVISAT ALTIMETRY Level 2 User Manual, 2011.
- Farrell, S. L., McAdoo, D. C., Laxon, S. W., Zwally, H. J., Yi, D., Ridout, A., and Giles, K.: Mean dynamic topography of the Arctic Ocean, *Geophysical Research Letters*, 39, <https://doi.org/10.1029/2011GL050052>, 2012.
- 35 Fecher, T. and Gruber, T.: Optimal Ocean Geoid as Reference Surface for Mean Ocean Circulation and Height Systems, in: EGU General Assembly Conference Abstracts, vol. 20 of *EGU General Assembly Conference Abstracts*, p. 8691, 2018.



- Förste, C., Bruinsma, S., Abrikosov, O., Lemoine, J.-M., Marty, J. C., Flechtner, F., Balmino, G., Barthelmes, F., and Biancale, R.: EIGEN-6C4 The latest combined global gravity field model including GOCE data up to degree and order 2190 of GFZ Potsdam and GRGS Toulouse, GFZ Data Services, <https://doi.org/10.5880/icgem.2015.1>, 2004.
- Greatbatch, R. J.: A note on the representation of steric sea level in models that conserve volume rather than mass, *Journal of Geophysical Research: Oceans*, 99, 12 767–12 771, <https://doi.org/10.1029/94JC00847>, 1994.
- Hayne, G.: Radar altimeter mean return waveforms from near-normal-incidence ocean surface scattering, *IEEE Transactions on Antennas and Propagation*, 28, 687–692, <https://doi.org/10.1109/TAP.1980.1142398>, 1980.
- Helland-Hansen, B. and Nansen, F.: The Norwegian Sea - Its Physical Oceanography Based Upon the Norwegian Researches 1900-1904, Report on Norwegian Fishery and Marine Investigations, Fiskeridirektoratets havforskningsinstitutt, <http://hdl.handle.net/11250/114874>, 1909.
- Hunke, E. and Dukowicz, J.: The Elastic-Viscous-Plastic Sea Ice Dynamics Model in General Orthogonal Curvilinear Coordinates on a Sphere-Incorporation of Metric Term, *Monthly Weather Review*, 130, 1848–1865, 2001.
- IHO, International Hydrographic Organization: Limits of Oceans and Seas, PANGAEA, Bremerhaven, 1953.
- Johannessen, J. A., Raj, R. P., Nilsen, J. E. Ø., Pripp, T., Knudsen, P., Counillon, F., Stammer, D., Bertino, L., Andersen, O. B., Serra, N., and Koldunov, N.: Toward Improved Estimation of the Dynamic Topography and Ocean Circulation in the High Latitude and Arctic Ocean: The Importance of GOCE, *Surveys in Geophysics*, 35, 661–679, <https://doi.org/10.1007/s10712-013-9270-y>, 2014.
- Koldunov, N. V., Serra, N., Köhl, A., Stammer, D., Henry, O., Cazenave, A., Prandi, P., Knudsen, P., Andersen, O. B., Gao, Y., and Johannessen, J.: Multimodel simulations of Arctic Ocean sea surface height variability in the period 1970–2009, *Journal of Geophysical Research: Oceans*, 119, 8936–8954, <https://doi.org/10.1002/2014JC010170>, 2014.
- Kvingedal, B.: Sea-Ice Extent and Variability in the Nordic Seas, 1967–2002, pp. 39–49, American Geophysical Union, <https://doi.org/10.1029/158GM04>, <http://dx.doi.org/10.1029/158GM04>, 2013.
- Kwok, R. and Morison, J.: Dynamic topography of the ice-covered Arctic Ocean from ICESat, *Geophysical Research Letters*, 38, <https://doi.org/10.1029/2010GL046063>, 2011.
- Kwok, R. and Morison, J.: Sea surface height and dynamic topography of the ice-covered oceans from CryoSat-2: 2011–2014, *Journal of Geophysical Research: Oceans*, 121, 674–692, <https://doi.org/10.1002/2015JC011357>, 2015.
- Large, W. and Yeager, S.: The global climatology of an interannually varying air-sea flux data set, *Clim. Dynam.*, 33, 341–364, <https://doi.org/10.1007/s00382-008-0441-3>, 2008.
- Laxon, S. W.: Sea-Ice Altimeter Processing Scheme at the EODC, *International Journal of Remote Sensing*, 15, 915–924, <https://doi.org/10.1080/01431169408954124>, 1994.
- Legeais, J.-F., Ablain, M., Zawadzki, L., Zuo, H., Johannessen, J. A., Scharffenberg, M. G., Fenoglio-Marc, L., Fernandes, M. J., Andersen, O. B., Rudenko, S., Cipollini, P., Quartly, G. D., Passaro, M., Cazenave, A., and Benveniste, J.: An improved and homogeneous altimeter sea level record from the ESA Climate Change Initiative, *Earth System Science Data*, 10, 281–301, <https://doi.org/10.5194/essd-10-281-2018>, 2018.
- Morison, J., Kwok, R., Peralta Ferriz, C., Alkire, M., Rigor, I., Andersen, R., and Steele, M.: Changing Arctic Ocean freshwater pathways, 481, 66–70, 2012.
- Mork, K. A. and Øystein Skagseth: Annual Sea Surface Height Variability in the Nordic Seas, pp. 51–64, American Geophysical Union (AGU), <https://doi.org/10.1029/158GM05>, 2013.



- Müller, F. L., Dettmering, D., Bosch, W., and Seitz, F.: Monitoring the Arctic Seas: How Satellite Altimetry Can Be Used to Detect Open Water in Sea-Ice Regions, *Remote Sensing*, 9, <https://doi.org/10.3390/rs9060551>, 2017.
- Orvik, K. A. and Niiler, P.: Major pathways of Atlantic water in the northern North Atlantic and Nordic Seas toward Arctic, *Geophysical Research Letters*, 29, <https://doi.org/10.1029/2002GL015002>, 2002.
- 5 Padman, L., Siegfried, M. R., and Fricker, H. A.: Ocean Tide Influences on the Antarctic and Greenland Ice Sheets, *Reviews of Geophysics*, 56, 142–184, <https://doi.org/10.1002/2016RG000546>, 2018.
- Pail, R., Fecher, T., Barnes, D., Factor, J. F., Holmes, S. A., Gruber, T., and Zingerle, P.: Short note: the experimental geopotential model XGM2016, *Journal of Geodesy*, 92, 443–451, <https://doi.org/10.1007/s00190-017-1070-6>, 2018.
- Parkinson, C. and Washington, W.: A Large-Scale Numerical Model of Sea Ice, *J. Geophys. Res.*, 84, 311–337,
10 <https://doi.org/10.1029/JC084iC01p00311>, 1979.
- Passaro, M., Cipollini, P., and Benveniste, J.: Annual sea level variability of the coastal ocean: The Baltic Sea-North Sea transition zone, *Journal of Geophysical Research: Oceans*, 120, 3061–3078, <https://doi.org/10.1002/2014JC010510>, 2015.
- Passaro, M., Rose, S. K., Andersen, O. B., Boergens, E., Calafat, F. M., Dettmering, D., and Benveniste, J.: ALES+: Adapting a homogenous ocean retracker for satellite altimetry to sea ice leads, coastal and inland waters, *Remote Sensing of Environment*,
15 <https://doi.org/10.1016/j.rse.2018.02.074>, 2018.
- Peacock, N. R.: Sea surface height determination in the Arctic Ocean from ERS altimetry, *Journal of Geophysical Research*, 109, C07 001, <https://doi.org/10.1029/2001JC001026>, 2004.
- Savcenko, R., Bosch, W., Dettmering, D., and Seitz, F.: EOT11a - Global Empirical Ocean Tide model from multi-mission satellite altimetry, with links to model results, <https://doi.org/10.1594/PANGAEA.834232>, 2012.
- 20 Schaffer, J., Timmermann, R., Arndt, J. E., Kristensen, S. S., Mayer, C., Morlighem, M., and Steinhage, D.: A global high-resolution data set of ice sheet topography, cavity geometry and ocean bathymetry, *Earth System Science Data Discussions*, 2016, 1–21, <https://doi.org/10.5194/essd-2016-3>, 2016.
- Scharroo, R. and Smith, W. H. F.: A global positioning system–based climatology for the total electron content in the ionosphere, *Journal of Geophysical Research: Space Physics*, 115, <https://doi.org/10.1029/2009JA014719>, a10318, 2010.
- 25 Serreze, M. and Barry, R.: *The Arctic Climate System*, Cambridge Atmospheric and Space Science Series, Cambridge University Press, <https://books.google.de/books?id=DjH6AwAAQBAJ>, 2014.
- Skourup, H., Farrell, S. L., Hendricks, S., Ricker, R., Armitage, T. W. K., Ridout, A., Andersen, O. B., Haas, C., and Baker, S.: An Assessment of State-of-the-Art Mean Sea Surface and Geoid Models of the Arctic Ocean: Implications for Sea Ice Freeboard Retrieval, *Journal of Geophysical Research: Oceans*, 122, 8593–8613, <https://doi.org/10.1002/2017JC013176>, 2017.
- 30 Smedsrud, L. H., Halvorsen, M. H., Stroeve, J. C., Zhang, R., and Kloster, K.: Fram Strait sea ice export variability and September Arctic sea ice extent over the last 80 years, *The Cryosphere*, 11, 65–79, <https://doi.org/10.5194/tc-11-65-2017>, <https://www.the-cryosphere.net/11/65/2017/>, 2017.
- Stade, E.: *Fourier Analysis*, John Wiley & Sons, Inc., <https://doi.org/10.1002/9781118165508>, 2005.
- Stammer, D., Ray, R. D., Andersen, O. B., Arbic, B. K., Bosch, W., Carrère, L., Cheng, Y., Chinn, D. S., Dushaw, B. D., Egbert, G. D., Erofeeva, S. Y., Fok, H. S., Green, J. A. M., Griffiths, S., King, M. A., Lapin, V., Lemoine, F. G., Luthcke, S. B., Lyard, F., Morison, J., Müller, M., Padman, L., Richman, J. G., Shriver, J. F., Shum, C. K., Taguchi, E., and Yi, Y.: Accuracy assessment of global barotropic ocean tide models, *Reviews of Geophysics*, 52, 243–282, <https://doi.org/10.1002/2014RG000450>, 2014.



- Steele, M., Morley, R., and Ermold, W.: PHC: a global ocean hydrography with a high-quality Arctic Ocean, *J. Climate*, 14, 2079–2087, [https://doi.org/10.1175/1520-0442\(2001\)014<2079:PAGOHW>2.0.CO;2](https://doi.org/10.1175/1520-0442(2001)014<2079:PAGOHW>2.0.CO;2), 2001.
- Vignudelli, S., Kostianoy, A. G., Cipollini, P., and Benveniste, J., eds.: *Coastal Altimetry*, Springer Berlin Heidelberg, <https://doi.org/10.1007/978-3-642-12796-0>, 2011.
- 5 Volkov, D. L. and Pujol, M.: Quality assessment of a satellite altimetry data product in the Nordic, Barents, and Kara seas, *Journal of Geophysical Research: Oceans*, 117, <https://doi.org/10.1029/2011JC007557>, 2012.
- von Appen, W.-J., Schauer, U., Hattermann, T., and Beszczynska-Möller, A.: Seasonal Cycle of Mesoscale Instability of the West Spitsbergen Current, *J. Phys. Oceanogr.*, 46, 1231–1254, <https://doi.org/10.1175/JPO-D-15-0184.1>, 2016.
- Wahr, J. M.: Deformation induced by polar motion, *Journal of Geophysical Research: Solid Earth*, 90, 9363–9368, <https://doi.org/10.1029/JB090iB11p09363>, 1985.
- 10 Wang, Q., Danilov, S., Sidorenko, D., Timmermann, R., Wekerle, C., Wang, X., Jung, T., and Schröter, J.: The Finite Element Sea Ice-Ocean Model (FESOM) v.1.4: formulation of an ocean general circulation model, *Geosci. Model Dev.*, 7, 663–693, <https://doi.org/10.5194/gmd-7-663-2014>, 2014.
- Wekerle, C., Wang, Q., von Appen, W.-J., Danilov, S., Schourup-Kristensen, V., and Jung, T.: Eddy-Resolving Simulation of the Atlantic Water Circulation in the Fram Strait With Focus on the Seasonal Cycle, *J. Geophys. Res. Oceans*, <https://doi.org/10.1002/2017JC012974>, 2017.
- 15 Zhang, Y. and Baptista, A.: SELFE: A semi-implicit Eulerian-Lagrangian finite-element model for cross-scale ocean circulation, *Ocean Modelling*, 21, 71–96, <https://doi.org/10.1016/j.ocemod.2007.11.005>, 2008.